The Cryosphere Discuss., 3, 33–75, 2009
www.the-cryosphere-discuss.net/3/33/2009/

The Cryosphere Discussions

The Cryosphere Discussions is the access reviewed discussion forum of *The Cryosphere*

Rapid and accurate measurement of the specific surface area of snow using infrared reflectance at 1310 and 1550 nm

J.-C. Gallet[1,2], **F. Domine**[1,2], **C. S. Zender**[1,3], **and G. Picard**[1,2]

[1]CNRS-INSU, Laboratoire de Glaciologie et Géophysique de l'Environnement, Saint-Martin d'Hères, France
[2]Université Joseph Fourier, Grenoble I, France
[3]Department of Earth System Science, University of California, Irvine, USA

Received: 17 November 2008 – Accepted: 26 November 2008 – Published: 21 January 2009

Correspondence to: F. Domine (florent@lgge.obs.ujf-grenoble.fr)

Published by Copernicus Publications on behalf of the European Geosciences Union.

Abstract

Even though the specific surface area (SSA) of snow is a crucial variable to determine the chemical and climatic impact of the snow cover, few data are available on snow SSA because current measurement methods are not simple to use in the field or do not have a sufficient accuracy. We propose here a novel determination method based on the measurement of the hemispherical reflectance of snow in the infrared using the DUFISSS instrument (DUal Frequency Integrating Sphere for Snow SSA measurement). DUFISSS uses 1310 and 1550 nm radiation provided by laser diodes, an integrating sphere 15 cm in diameter, and InGaAs photodiodes. For SSA<60 $m^2 kg^{-1}$, we use the 1310 nm radiation, reflectance is in the range 15 to 50% and the accuracy is 10%. For SSA>60 $m^2 kg^{-1}$, snow is usually of low to very low density (typically 30 to 100 $kg m^{-3}$) and this produces artifacts caused by the *e*-folding length of light in snow being too long. We therefore use 1550 nm radiation for SSA>60 $m^2 kg^{-1}$. Reflectance is then in the range 5 to 12%, and the accuracy is 12%. No effect of crystal shape on reflectance was detected. We propose empirical equations to determine SSA from reflectance at both wavelengths, with that for 1310 nm taking into account the snow density. DUFISSS has been tested in the Alps to measure the snow area index (SAI) of the Alpine snowpack in a south facing area at 2100 m elevation. This was done by measuring the SSA, thickness and density of the seven main layers of the snowpack in just 30 min, and a value of 5350 was found, significantly greater than in Arctic and subarctic regions. DUFISSS can now be used to help study issues related to polar and Alpine atmospheric chemistry and climate.

1 Introduction

Snow is a porous medium that strongly impacts the energy budget of the Earth (Warren, 1982; Hall, 2004) and the chemistry of the lower troposphere (Domine and Shepson, 2002; Grannas et al., 2007). The physical property of snow that contributes the most to

these impacts is probably its specific surface area (SSA). Snow SSA is defined as the surface area per unit mass (Legagneux et al., 2002), i.e. SSA=$S/\rho_{ice}V$, where S is the surface area of a given mass of snow particles, V is the volume of the snow particles, and ρ_{ice} is the density of ice (917 kg m^{-3} at 0°C). SSA values range from 2 m^2 kg^{-1} for melt-freeze layers to 156 m^2 kg^{-1} for fresh dendritic snow (Domine et al., 2007a).

Light scattering by snow is determined by its SSA. Grenfell and Warren (1999) showed that the albedo of non-spherical particles could be well represented by a collection of independent spheres having the same S/V ratio as the particles, demonstrating that SSA was a crucial variable to model snow optics, and therefore the energy budget of snow-covered surfaces. For example, using the DISORT radiative transfer model of Stamnes et al. (1988), we calculated light transmission through the troposphere and in the snowpack, and found that a reduction in SSA of snow from 32 to 16 m^2 kg^{-1} at the summer solstice at noon, 65° N, would cause an instantaneous forcing of 22 W m^{-2} at the tropopause, increasing column solar absorption by about 6.5%.

Because of its porous nature, the snowpack adsorbs large amounts of volatile and semi-volatile chemical species. In particular the uptake of persistent organic pollutants (POPs) by the snowpack from the atmosphere has generated considerable interest (Daly and Wania, 2004; Herbert et al., 2005; Domine et al., 2007b, Burniston et al., 2007). If the surface coverage of an adsorbed POP remains significantly less than a monolayer, its concentration in snow, $[POP]_{snow}$, can be expressed as a function of snow SSA, of the partial pressure of the POP, P_{POP}, and of temperature T, according to Domine et al. (2007b):

$$[POP]_{snow} = P_{POP} \times SSA/H_{POP}(T) \quad (1)$$

where $H_{POP}(T)$ is the surface Henry's law constant at the snow temperature, expressed in Pa m^2 mol^{-1}, while $[POP]_{snow}$ is in mol kg^{-1}. The knowledge of SSA is therefore essential to quantify POP concentrations in snow.

The chemical impact of snow is not limited to the adsorption of species. Photochemical reactions also take place in snow, and the photolysis of the nitrate ion in snow,

resulting in the emission of NO and NO_2 to the atmosphere, has been the subject of numerous studies (Honrath et al., 1999; Jones et al., 2001; Beine et al., 2002). If it is assumed that nitrate ions are adsorbed on the surface of snow particles, a subject of debate (Beine et al., 2006; Jacobi and Hilker, 2007; Grannas et al., 2007) then the rate of nitrate photolysis also depends on snow SSA, as detailed in Domine et al. (2008).

Despite the importance of snow for both the energy budget of the Earth, and therefore climate, and atmospheric chemistry, and despite the fact that knowing snow SSA is crucial to evaluate quantitatively both aspects, very few data are available on snow SSA. Furthermore, snow SSA changes with time because of snow metamorphism (Flanner and Zender, 2006; Taillandier et al., 2007), but many aspects of its rate of change are not elucidated. This is because we are today lacking a rapid and accurate method to measure snow SSA. This has impeded both the measurement of snow SSA in studies motivated by climate and chemistry issues, and the study of the rate of change of snow SSA in the field and during cold room experiments.

Most SSA measurements to date have been done using methane adsorption at 77 K (Legagneux et al., 2002; Domine et al., 2007a). Briefly, snow placed in a vacuum container is immersed in liquid nitrogen and the adsorption isotherm of methane on snow is measured, allowing the determination of snow SSA. While this method is reliable and accurate, with a reproducibility of 6%, obtaining one value take three hours and requires liquid nitrogen, a problem in field studies. Another method is stereology (Narita, 1971). Briefly, a snow block is filled with a water-insoluble liquid that freezes at $T<0^{\circ}$C to harden it. Polishing the sample produces serial sections (Perla et al., 1986) that are photographed. The images are then analyzed (Davis et al., 1987) to yield a SSA value after about four hours of work. This method is also well established, but does not work well for fresh snow with high SSA, which cannot be manipulated easily, and because images often lack the resolution needed to detect very small structures. Lastly, X-ray tomography can also produce SSA values (Flin et al., 2003; Kerbrat et al., 2007) but this is not easy to use in the field and the method does not have a sufficient resolution to be used for fresh snow (Kerbrat et al., 2008).

Theory predicts that the reflectance of snow, R_s, depends on snow grain size and therefore on snow SSA (Warren, 1982; Grenfell and Warren, 1999). By measuring simultaneously the spectral reflectance and the SSA of snow samples, Domine et al. (2006) have verified experimentally that in the short wave infrared (SWIR, 1300 to 3000 nm), most variations in snow reflectance could be explained by variations in snow SSA, in good agreement with theory. Theory also predicts that grain shape affects reflectance (Kokhanovsky, 2006; Picard et al., 2008) but this appeared to be a second order effect in the study of Domine et al. (2006). Those authors also showed plots of R_s=f(SSA) for several wavelengths between 1310 and 2260 nm, and suggested that reflectance measurements in that range could be used for SSA determination. Matzl and Schneebeli (2006) used near infrared (NIR) reflectance around 900 nm to determine SSA vertical profiles in a snow pit with a camera, the SSA-R_s calibration being done with stereological measurements. The interest of that method is that it yields vertical SSA profiles rapidly. Painter et al. (2007) also designed an optical system to rapidly measure snow reflectance around the absorption line at 1030 nm, from which they deduced optical grain size, rather than SSA, using the modeling approach of Nolin and Dozier (2000).

While both these techniques have enormous potential for stratigraphic studies, they can be improved by operating at longer wavelengths and with an improved control of the illumination. Reflectance is indeed less dependent on SSA in the NIR than in the SWIR, and it is not clear what accuracy can be obtained in both above studies. Moreover, the SSA-reflectance relationship is not linear, with the result that determining SSA from reflectance is less accurate at high SSA values, and this problem worsens rapidly at shorter wavelengths (Domine et al., 2006). This may render the monitoring of the evolution of the SSA of fresh snow difficult. Since fresh snow SSA evolves rapidly (Cabanes et al., 2002, 2003; Taillandier et al., 2007), this is where the exchange of energy and adsorbed species with the atmosphere will change the most rapidly, and there is therefore the need for an accurate determination of snow SSA, that will be efficient over the whole range of SSA encountered in seasonal snowpacks and near

the surface of ice caps.

Another drawback of working at wavelengths around 900–1000 nm is that the *e*-folding depth of light in snow is fairly large. We calculate using the DISORT optical transfer model of Stamnes et al. (1988) that at 900 nm, for snow of SSA=35 $m^2\,kg^{-1}$ and density=200 $kg\,m^{-3}$, the snow thickness needed to obtain 99% of the reflectance at infinite thickness is 3.9 cm. This may cause interferences between layers, that could be reduced by using wavelengths were ice is more absorbing. For example, at 1310 nm, the *e*-folding depth of that same snow is reduced to 1.1 cm, and this is further reduced to 0.2 cm if 1550 nm radiation is used.

Since snow is not a lambertian reflector, R_s measured in many previous studies are not directly comparable with the albedo, i.e. the integrated hemispherical reflectance. Domine et al. (2006) measured bidirectional reflectance at a single configuration. The illumination came from the sun with a high solar zenith angle and the viewing angle was at nadir. In Painter et al. (2007), the source and the receiver are fixed at 23° and 35° zenith angles, respectively. However, since the system is surrounded with a hemispherical reflector, multiple scattering between the snow wall and this reflector may be significant. Therefore, the total illumination on the snow is not perfectly direct but partially diffuse. In the photography technique of Matzl and Schneebeli (2006), the viewing angle was normal to the wall but the illumination came from the sun and clouds and was diffused by a cloth laid over the snowpit and by the 4 faces of the snowpits. It was therefore partially diffuse, dominantly downward and possibly heterogeneous (Matzl and Schneebeli, 2006).

These different optical configurations make intercomparisons between the various systems used difficult at best. Moreover, the non-lambertian character of snow and its complex bi-directional reflection distribution function (BRDF, Grenfell et al., 1994) imply that R_s may strongly depend on grain shape. Measuring the hemispherical instead of the bi-directional reflectance is recommended to measure SSA accurately because hemispherical reflectance is better related to the optical diameter (equivalent of the SSA in terms of optics) than the bi-directional reflectance (Grenfell and Warren,

1999) and it is less affected by grain shape. A stable and reproducible illumination is also important for the reproducibility of measurements, which excludes the sun as the illumination source.

We report here the development of a novel optical system (DUFISSS: Dual Frequency Integrating Sphere for Snow SSA measurements) to measure snow reflectance at 1310 and 1550 nm, the shorter wavelength being optimal for SSA<60 $m^2 kg^{-1}$ while the longer one is more efficient for SSA>60 $m^2 kg^{-1}$. To measure the hemispherical reflectance, we used an integration sphere that collects light reflected by the snow in all directions. The signal was found to depend on SSA but also on density, so that modeling approaches were required to test and quantify the effect of density. The calibration of the SSA-reflectance relationship was done using methane adsorption. This new optical system allows one SSA value to be determined in the field in about one minute, and it successfully operates outdoors in polar conditions.

2 Experimental apparatus

The system used is shown in Fig. 1. Its main component is a 15 cm inner diameter (i.d.) integration sphere from Sphere Optics made of Zenith®, a polymer with a nominal reflectance near 0.985 in the SWIR. The snow sample is placed in a black sample holder 63 mm i.d. and 13 or 25 mm deep. The opening in the sphere towards the snow sample is 38 mm in diameter. The snow is illuminated directly by the collimated beam from a laser diode at 1310 or 1550 nm (both supplied by Mitsubishi, and of nominal power 6 mW). The beam diameter used is about 10 mm at 1310 nm. At 1550 nm, we initially used a beam diameter of 4 mm, later increased to 8 mm. The beam diameter chosen is a compromise between illuminating a representative area and minimizing the numbers of photons hitting directly the sphere. The outside of the sphere in contact with the snow (Fig. 1) is black, with a reflectance of 3% in the SWIR. Light reflected by the snow is collected by an InGaAs photodiode, whose current is converted to voltage and amplified before measurement by a high precision voltmeter. Reflectance stan-

dards made of graphite-doped Zenith®, supplied and calibrated by Sphere Optics, are used to determined the reflectance from the photodiode signal. The calibration curve of the photodiode signal is shown in Fig. 2. It is not linear because the sample is re-illuminated by light diffused by the snow and reflected back by the sphere surface. The equation used to fit the calibration curve is described when we discuss the contributions to snow reflectance in more detail in Sect. 3. Calibration of the reflectance signal to determine SSA was done by measuring successively the snow reflectance, its SSA using methane adsorption, and its reflectance again to detect any change in SSA caused by manipulating the snow.

As mentioned above, crystal shape also affects reflectance. Picard et al. (2008) modeled the reflectance of snow crystals of different model shapes (spheres, cubes, cylinders, etc.) using a ray-tracing method at 1310 nm and observed that for a given SSA, reflectance could vary within ±25% by changing the crystal shape. This contrasts with the experimental data of Domine et al. (2006) who however studied only 12 samples. To further investigate this crucial issue, the snow samples that we used in the SSA-reflectance calibration therefore had a wide range of shapes and included highly faceted depth hoar, rounded grains, needles and fresh dendrites. Photographs of such snow types can be found in Domine et al. (2008) and Taillandier et al. (2007).

Two aspects of the reproducibility of our reflectance measurements were determined. The first one was the reproducibility of the measurement of a given snow sample placed in a given sample holder. This was done by placing the sample under the sphere, then removing it and replacing it after a random rotation about a vertical axis. Variations were within 0.3% at 1310 nm and 1.5% at 1550 nm. The second one was to fill the sample holder with snow from one layer sampled in the field in a large container, homogeneized by mixing, and taken to our cold room. The sample-holder container was then emptied and refilled with new snow from the same container. Heterogeneities in the snow layer as well as variations in the way snow was manipulated may then cause signal variations. In that second case, variations were within 1% at 1310 nm and 2% at 1550 nm, showing that our reflectance measurements are highly

reproducible.

The SSA-reflectance calibration data at 1310 nm is shown in Fig. 3. While for SSA<66 $m^2\,kg^{-1}$, the data show the expected trend (Domine et al., 2006), we see that for SSA>66 $m^2\,kg^{-1}$, reflectance values show a lot of scatter and are much lower than expected from an extrapolation of the data at lower SSA: the maximum reflectance is 56.2%, obtained for a SSA of 131.3 $m^2\,kg^{-1}$, and that value is barely higher than 54.4%, obtained for a sample of SSA 65.3 $m^2\,kg^{-1}$. Since all these snows with high SSA also had a low density, we realized that the geometry of our system could produce artifacts of two kinds, shown in Fig. 4:

- The *e*-folding depth of light (i.e. the depth over which the transmitted light intensity is reduced by *e*) can become sufficient in low density snow so that a significant amount of light reaches the bottom of the black sample holder, where it is absorbed (hereafter: density artifact). Initially, we used a 13 mm-deep sample holder (reflectance 3% in the SWIR), subsequently replaced with a 25 mm-deep one (reflectance 6% in the SWIR) to reduce this effect.

- Even if light does not reach the sample holder, light reflected by crystals at a depth z below the snow surface will have an effective solid angle where reflected light can escape from the sample holder that is lower that for a snow crystal located near the surface, where the effective solid angle is in principle 2π steradians (hereafter: geometric artifact).

Quantifying these effects and correcting them to obtain a calibration curve that would be simple to use required modeling, detailed in Sect. 3. Another option that we pursued after becoming aware of these artifacts was to use a wavelength whose *e*-folding length was lower than at 1310 nm, in order to minimized those artifacts. Given commercially available diode lasers, we selected 1550 nm, and the relevant results are detailed in Sect. 4.

3 Reflectance modeling and correction methods

3.1 Modeling using DISORT

Our first modeling approach used the DISORT code of Stamnes et al. (1988) in conjunction with snow grain optical properties from Mie theory. This method approximates snow crystals as disconnected spheres and models the reflection of diffuse and directional light by a discrete number of snow layers of finite thickness but infinite in the horizontal direction. To reduce biases due to discretization and resonance effects (e.g. Zender and Talamantes, 2006), we represent snow crystals as a log-normal distribution of spheres. The reflectance depends slightly on the exact distribution chosen. Since DISORT models disconnected spheres and not real snow, perfect agreement between calculations and experiments is not expected. To optimize the agreement, we chose to adjust the size distribution and the ice optical constants. In all cases we used a log-normal distribution with σ=1.6, as observed in Antarctica by Grenfell and Warren (1999), and that resolves all sizes between 0.2 and $5r_{eff}$, where $r_{eff}=3/(\rho_{ice}\mathrm{SSA})$ is the optical radius. At 1310 nm, the ice optical constant used was $n_{1310}=1.29584+i1.302\times10^{-5}$, based on the compilation of Warren and Brandt (2008). The real part used is that of the compilation. For the imaginary part, the compilation value is 1.310×10^{-5} at −7°C but there is a 2% experimental uncertainty and an unquantified temperature dependence, so our value appears reasonable. At 1550 nm, the optical constant used was $n_{1550}=1.2907+i4.586\times10^{-4}$. The real part is that of Warren and Brandt (2008). For the imaginary part, Gosse et al. (1995) recommend 4.26×10^{-4} at −22°C, with an error of 3% and a temperature dependence of 0.6% K^{-1} (Warren and Brandt, 2008), so that our value is within the acceptable range.

In our sphere, illumination is by direct light with normal incidence, but the snow is re-illuminated by diffuse light reflected from all over the sphere surface. Snow reflectance depends on the angle of incidence, because snow mostly forward-scatters light (Warren, 1982) and therefore the probability that a photons exits the snow is lowest for normal incidence. Modeling snow reflectance in our system therefore requires

the estimation of the amount of diffuse light hitting the snow. The photon distribution in an ideal integrating sphere evolves as a Markov process (Pickering et al., 1993). We adapted the simple yet accurate Markov model presented and evaluated in Hidović-Rowe et al. (2006) to our experimental geometry. The model assumes that the snow surface is flat and Lambertian. It also accounts for the optical baffle which blocks the detector from specular reflection (Fig. 1). Adopting the terminology of Hidović-Rowe et al. (2006), we can express the diffuse downwelling radiation $f_d^{\downarrow}$ as a fraction of the incident direct beam,

$$f_d^{\downarrow} = \frac{\dot{r}\omega\alpha s}{1-(s+d)-\omega\alpha\{1-[d+(1-r)s]\}} \quad (2)$$

where $\dot{r}$ is the snow reflectance to direct normal radiation, and ω and r are the reflectances of the sphere wall and the snow to isotropic illumination, respectively. The remaining parameters are the normalized surface areas of the sphere walls (α=0.981642), photodiode (d=0.000145), and snow sample (s=0.015877). The normalized surface area of the laser diode, h, is 0.002336, so that $\alpha+s+d+h=1$.

We observed, however, that the signal was higher than expected in the absence of a sample or in the presence of a very dark reflector in place of the sample, indicating that the beam collimation was not perfect and that some photons hit the sphere walls directly. Correcting Eq. (1) to account for emission fractions $\dot{f}$ and $1-\dot{f}$ initially striking the sample (collimated photons) and the sphere walls (stray photons), respectively, yields

$$f_d^{\downarrow} = \omega s \frac{\dot{f}\dot{r}\alpha + \{1-\dot{f}\}[1-(s+d)]}{1-(s+d)-\omega\alpha\{1-[d+(1-r)s]\}} \quad (3)$$

The signal expected to be measured at the photodiode is:

$$m = \omega d \frac{\dot{f}\dot{r}\alpha + \{1-\dot{f}\}[1-(s+d)]}{1-(s+d)-\omega\alpha\{1-[d+(1-r)s]\}} \quad (4)$$

Equation (4) was used to fit the calibration curves of Fig. 2. In that case, we assume that the standards are lambertian reflectors, and Eq. (4) is simplified because $\dot{r}=r$. The value of $\dot{f}$ had to be adjusted for every calibration, and in particular when the laser diode or its collimation (beam width) was changed. We also found that the fits were best with $\omega_{1310}=0.972$ and $\omega_{1550}=0.965$, while the manufacturer mentioned slightly higher values. The fitted calibration curves were then used to determine the reflectance of the snow samples from the photodiode signal.

Figure 3 also shows a SSA-Reflectance theoretical curve calculated for lighting conditions prevailing in the sphere, using DISORT and Eq. (3) to account for diffuse light reflected by the snow. We used a horizontally infinite 25 mm-thick snow layer of density 400 kg m^{-3} (the effect of density levels off in all cases for values >200 kg m^{-3}), made of disconnected spheres and underlaid by a dark surface (6% reflectance for the 25 mm sample holder). We also used $\dot{f}=0.95$. The value of $\dot{f}$ in fact has little impact on the calculated reflectance at 1310 nm. For example, for SSA=40 m^2 kg^{-1}, reflectance is 46.081% for $\dot{f}=0.9$ and 45.807% for $\dot{f}=1$. Figure 5 shows quantitatively the difference between calculated and measured reflectances, for the SSA values obtained by CH_4 adsorption. For SSA<66 m^2 kg^{-1}, the data are reproduced fairly well. There is scatter of ±10% for a number of points with SSA around 20 m^2 kg^{-1}.

It is tempting to attribute this difference to grain shape. However, some of these points were obtained from samples with rounded grains, while others are from depth hoar, and for the moment we have not detected experimentally any correlation between grain shape and reflectance. These low SSA samples all had large grains, and it was difficult to obtain a smooth sample surface. Some surfaces had hollows, while others had grains sticking out of the surface. Given the geometric artifact discussed above, it is clear that this affected the reflectance, and we suggest that this uneven sample surface is the main reason for the difference between experiment and theory. In Fig. 5, a cluster of points with SSA around 60 m^2 kg^{-1} shows excellent agreement between theory and experiment, because the grains were much smaller and it was easier to obtain a smooth surface.

For SSA>66 $m^2\,kg^{-1}$, the calculated reflectance is systematically greater than the measured value, and the difference is about 16% for SSA>75 $m^2\,kg^{-1}$. To test whether density effects could explain the gap between our theoretical curve and the data for SSA>75 $m^2\,kg^{-1}$ we modeled with DISORT the reflectance of these samples using their measured densities. Table 1 compares the experimental data to calculations. Comparison of both calculated values show that density accounts for differences in reflectance of less than 1%. This shows that the gap between the experimental points with SSA>75 $m^2\,kg^{-1}$ and the theoretical curve of Fig. 3 cannot be explained by density effects alone.

To assess the contribution of the geometric artifact to hemispherical surface albedo A_s, we modeled A_s as the sum (over all snow layers) of the product of two independent terms for each layer: the mean field-of-view (FOV, measured in hemispheres) subtended, and the albedo contribution A_k predicted by plane-parallel radiative transfer theory. We approximated the geometric correction due to finite horizontal and vertical sample dimensions as Eq. (5), the sum of layer-dependent geometric factors (FOV_k) times the corresponding plane-parallel layer albedo contribution (A_k). These factors are intuitive and predictable for all wavelengths with standard methods.

$$A_s = \sum_k FOV_k A_k \tag{5}$$

The snow was discretized on a 32-layer vertical grid stretching in layer thicknesses from 10 µm near the top to 2.5 mm near the bottom. On this grid, no layer contributes more than 10% to A_s. For each layer, we calculated the mean solid angle of the integrating sphere subtended by each snow layer. Snow farther from the central axis of the sample container subtends a smaller planar angle ψ of the aperture (Fig. 4b), and occupies a greater relative surface area than snow nearer the central axis. The average layer FOV is estimated as the surface-area mean FOV of all snow extending out to the radius of illumination. Note that the FOV determined in this way is geometric only; it does not account for attenuation and scattering. The FOV of diffusely illuminated snow

decreases from 1.0 to 0.43 to 0.2 hemispheres as snow depth increases from 0 to 13 to 25 mm. The FOV depends on whether the beam is collimated or whether illumination is diffuse. At 25 mm depth, the mean FOV for snow illuminated by the collimated beam (~10 mm diameter) exceeds that of snow diffusely illuminated across the entire aperture by about 6%.

The plane-parallel prediction of each layer's contribution to albedo A_k was constructed by applying the adding method to the delta-Eddington approximation of snow sample optical properties. After first discretizing the (presumably) homogeneous snow sample into 32 layers, the procedure of Coakley et al. (1983) was used to determine and add the optical properties for each layer. We treat the sample holder bottom as an additional layer with reflectance 6% and transmittance 0% in order to determine its contribution to albedo. At 1310 nm, the surface albedo in the 13 mm sample holder is within about 2.5% of the albedo of a semi-infinite layer, A_∞, of bright snow of low density (50 kg m^{-3}, SSA=100 m^2 kg^{-1}). For the 25 mm sample holder, or for fresh snow of higher density (>100 kg m^{-3}), A_s deviates from A_∞ by <0.1%. We estimate that the absorbing lower boundary reduces the measured reflectance of the samples in Table 1 by less than 1% from their semi-infinite value. The geometric correction (5) results in relative reduction of the plane-parallel modeled albedo A_s for the samples shown in Table 1 by 6.6%, 7.2%, 7.6%, 2.8%, and 4.1%, respectively. Hence this geometric correction reduces the bias between the measured and plane-parallel modeled albedos in Table 1 by 25–50%. At the same time, the geometric correction reduces A_s by less than ~1% for denser snow (>200 kg m^{-3}) with moderately high SSA (~66 m^2 kg^{-1}).

Figure 6 shows that for those low density samples with SSA>66 m^2 kg^{-1}, these corrections only account for less than half of the difference between the reflectance values measured and those calculated by DISORT. We believe that this is because our corrections and DISORT cannot take into account the complex path taken by rays of light in the sample. Our correction method hypothesizes that if a given areal fraction of a given snow layer is illuminated, the fraction of scattered light that will escape the sample can be predicted by simple geometric considerations. However, the three-dimensional

sample geometry causes edge effects that are not captured by the one-dimensional multiple scattering algorithm (DISORT) or by our geometric corrections. We conclude that plane-parallel optical models, even with corrections, are inadequate for quantitative treatment of bright, low-density snow reflectance in DUFISSS.

3.2 Modeling using a ray-tracing model

The other approach pursued was to use the ray-tracing method of Picard et al. (2008) to obtain theoretical calibration curves for various snow densities. Picard et al. (2008) showed that snow reflectance was highly dependent on crystal shape. For example, for a given SSA, the reflectance of cubes was 27% greater than that of disconnected spheres, as used in DISORT. However, for SSAs lower than 66 $m^2\,kg^{-1}$, this large dependence is not reproduced by our data, which do not show much scatter around the DISORT theoretical curve, calculated using disconnected spheres (Fig. 3). We suggest that this is due to the fact that natural snow always contains a mixture of a wide range of shapes. Indeed, except perhaps for surface hoar, snow is never formed of only faceted crystals. This is because faceted shapes are caused by rapid growth, which is fed by the sublimation of other crystals, and sublimation always produces rounded shapes (Nelson, 1998). Figure 7 shows a depth hoar crystal, with the obvious and typical coexistence of both faceted and rounded shapes. Likewise, snow is rarely if ever formed of only rounded shapes. Melt-freeze crusts are generally thought to consist only of rounded shapes. However, Fig. 7 also shows a melt-freeze crust, and although rounded shapes predominate, faceted forms are commonly found. We speculate that these could be formed either in localized environments where latent heat release produced large water vapor fluxes or because these melt-freeze crusts were subjected to strong transient temperature gradients that produced rapid growth after the melting event. Snow subjected to perfectly isothermal conditions is also commonly thought to consist only of rounded shapes (Colbeck, 1983). However, using scanning electron microscopy, Domine et al. (2003) showed that even in such snow, facets were formed. In summary, we suggest that natural snow is almost always made of a variety of shapes

that will considerably reduce the dependence of hemispherical reflectance on snow crystal shape as discussed by Picard et al. (2008).

We therefore applied a modified version of the ray-tracing model of Picard et al. (2008), SNOWRAT, to which we added a representation of the integrating sphere and computed the reflectance of the snow samples having the SSA values shown in Fig. 6, treating the snow as disconnected spheres. SNOWRAT does not treat stray photons, so that $\dot{f}=1$. This can produce a systematic bias in the data, but so can the arbitrary selection of spheres as crystal shape. We therefore need to remain aware of such a possible systematic bias when interpreting SNOWRAT results, which have been added to Fig. 6. While the geometric correction always undercorrected DISORT reflectances, Fig. 6 shows that the differences between measured and SNOWRAT values at first sight appear random. A closer look shows that SNOWRAT underestimates reflectance for snow of very low density (33–41 $\mathrm{kg\,m^{-3}}$) and overestimates reflectance for snow of low density (86–109 $\mathrm{kg\,m^{-3}}$).

The impact of density on ray-tracing-derived reflectances was therefore tested. Figure 8 shows calculations of the reflectances of snow samples of SSA=110 $\mathrm{m^2\,kg^{-1}}$ of various densities. The measured reflectance of a snow sample with the same SSA is also shown. As density is increased from 27 to 45 $\mathrm{kg\,m^{-3}}$, the reflectance increases dramatically, from 43 to almost 53%. This demonstrates that in our system, the measured reflectance is extremely sensitive to density for low density values. We believe that this may explain the differences between measured and ray-tracing-derived reflectances in Figs. 6 and 8. Experimentally, the density of our samples are measured simply by weighing the sample holder filled with snow and this of course only measures the mean density in the sample holder. For reflectance measurements, the sample holder is scraped after being filled with snow, to obtain a flat level surface. This probably affects the density of the surface layer, which is then different from the mean density. Figure 6 suggests that when the density if very low, our sample handling increases the density of the surface layer, while the opposite is observed when the density is somewhat higher. Figure 8 also plots a measured value, whose reflectance is

about 6.5% higher than calculations. This is consistent with calculations that show that reflectance is highly sensitive to density and with our suggestion that the mean density may not reflect density variations within the sample, so that predicting reflectance from the mean density is prone to large errors. Moreover, as mentioned above, simulating snow crystals as spheres may also produce a bias.

Figure 9 shows a plot of the effect of density on the reflectance of snow of low SSA: 28 $m^2\,kg^{-1}$. Such snows are denser than high SSA snows, and the density range chosen here is 145–270 $kg\,m^{-3}$. Figure 9 shows that over this range, reflectance only varies between 35.25 and 37.60%, and these extreme values include numerical noise, i.e. noise caused by an insufficient number of light rays used (1 million) because of limitations in computer ressources, which results in imperfect convergence. Therefore, actual meaningful variations in calculated reflectance are probably within 1%. The measured reflectance of a snow sample with SSA=28.1 $m^2\,kg^{-1}$ is also shown, and is 38.9%, within 1.5% of the calculated value. The facts that at moderate SSA and density, reflectance weakly depends on density and that calculated and measured reflectances are close indicate that determining SSA from reflectance for such snows is possible. However, the data of Fig. 8 lead to the inescapable conclusion that, given the density dependence of reflectance for snow of low density and high SSA, and given the fact that fresh snow of high SSA almost always has a low density, our integration sphere with illumination at 1310 nm is not adapted to the measurement of the SSA of low density-high SSA snow. For such snows, we must find a method where reflectance is less affected by density.

4 Determination of high SSA values from reflectance at 1550 nm

Density causes an artifact when 1310 nm radiation is used because radiation penetrates too deep in the snow. For example, we calculate using DISORT that for snow with SSA=100 $m^2\,kg^{-1}$ and density=50 $kg\,m^{-3}$, a snow thickness of 23 mm lying over a surface with 6% reflectance is needed to get 99% of the reflectance at infinite thick-

ness. Given the artifacts shown in Fig. 4, it is inevitable that this required thickness will cause erroneous SSA determinations. By using a wavelength that is more strongly absorbed by ice, the penetration depth can be reduced and artifacts can be minimized. If however absorption is too important, the reflectance signal will be too low, reducing accuracy. Given commercially available laser diodes, the best compromise that we found was to use 1550 nm radiation.

Figure 10 shows the SSA-reflectance calibration data at 1550 nm. As before, the reflectance at 1550 nm (and also at 1310 nm) was measured, followed by a SSA measurement using CH_4 adsorption at 77 K, and by a second reflectance measurement at both wavelengths. Only snow samples with high SSAs, and therefore low densities, were selected for these measurements. Figure 10 also shows calculations using DISORT, without geometric corrections. At 1550 nm, calculated reflectances were found to show a significant dependence on $\dot{f}$. This is because at 1550 nm snow reflectance is low, usually <10%, so that the ratio of direct/diffuse flux (i.e. collimated/stray photons) is higher at 1550 nm than at 1310 nm. Figure 10 therefore shows 3 curves for the $\dot{f}$ values corresponding to those used in the experiments. This trend is also detected in the experimental data, as snow reflectances measured with $\dot{f}\approx 0.81$ are slightly higher than for $\dot{f}\approx 0.94$. For SSAs in the range 58–93 $m^2\,kg^{-1}$, with densities in the range 35–178 $kg\,m^{-3}$, our experimental points coincide well with the predictions of DISORT. However, for the five samples whose SSAs fall in the range 107–131 $m^2\,kg^{-1}$, with densities in the range 33–41 $kg\,m^{-3}$, measured reflectances are slightly lower than calculated by DISORT.

It is essential to test whether these differences are simply due to experimental error or whether they are caused by the low density of the snows. Indeed, opportunities to obtain snow with SSA>100 m^2kg^{-1} are not very frequent, and random errors in the 5–10% range for these five data points could explain the difference. Figure 11 shows the effect of density on reflectance at 1550 nm, as calculated by the ray-tracing model. The variations appear to be within numerical noise, and density effects on reflectance at 1550 nm can then be neglected.

To confirm this, Fig. 12 compares measured reflectances to those calculated using SNOWRAT, DISORT, and DISORT with the geometric correction. This is similar to the calculations at 1310 nm, shown in Fig. 6. The differences between the measurements and SNOWRAT predictions are between 0.01 and 0.53% of reflectance in absolute value and are random, consistent with the absence of a detectable density effect. The geometric correction is too small to correct the systematically too bright DISORT bias. Although we realize that the number of data points available at very high SSA is limited, we conclude for the moment that the deviation of the calibration points from theory at very high SSA, shown in Fig. 10, is due to experimental error and not to an effect of density.

5 Recommendations to determine SSA from reflectance

The above experimental and modeling data indicate that snow SSA can be determined rapidly and accurately in the field using DUFISSS and the following recommendations.

5.1 Recommendation for snow with SSA<60 $m^2\,kg^{-1}$

For snow with SSA<60 $m^2\,kg^{-1}$, we recommend the use of 1310 nm radiation. If the grains are large, this may result in surface roughness and potential large error on reflectance. We recommend measuring several samples from the same layer, so that averaging several sample surfaces will reduce errors. We recommend the use of the DISORT curve of Fig. 3, valid without correction for densities ρ>200 $kg\,m^{-3}$. To facilitate the use of Fig. 3, we propose the following polynomial fit, with SSA in $m^2\,kg^{-1}$ and reflectance A_s in %:

$$\mathrm{SSA} = 1.739\times10^{-7}A_s^5 - 1.633\times10^{-5}A_s^4 + 8.166\times10^{-4}A_s^3 - 0.01081A_s^2 + 0.4508A_s + 0.03519 \quad (6)$$

Even though we recommend Eq. (6) for SSA<60 $m^2\,kg^{-1}$, we are fairly confident that

it can be used in the range $1<SSA<66\,m^2\,kg^{-1}$, as suggested by Fig. 3. For the same SSA range, but for $50<\rho<200\,kg\,m^{-3}$, we recommend taking into account the effect of density, ρ. To derive an empirical equation that takes into account density, we used the data of Fig. 9 and additional SNOWRAT calculations performed for $SSA=60\,m^2\,kg^{-1}$, shown in Fig. 13. From those data, we propose to replace the measured reflectance A_s with a corrected value $A_{s,corr}$:

$$A_{s,corr} = \frac{A_s(2000 + 0.986\rho^{2.25})}{\rho^{2.25}} \quad (7)$$

and to use $A_{s,corr}$ in Eq. (6) to obtain the SSA. Equation (7) has no theoretical basis, it is purely empirical and its only merit and purpose are to reproduce our data and calculations. Many other forms of equations could be proposed, all with the same arbitrary character.

The error on SSA can be evaluated. The reflectance standards have an absolute accuracy of 0.6%, determined by the manufacturer. An individual SSA measurement using CH_4 adsorption has a random error of 6% (Legagneux et al., 2002). The relevant part of the calibration curve in Fig. 3 uses 34 points, and we estimate that the error done by using this curve is 4%. The random error of one reflectance measurement is 1%, as detailed in section 2. Despite the fact that we could not detect any significant effect on snow crystal shape on reflectance, there is a clear possibility that this effect does exist, and we estimate that this effect may produce an error of 3% on SSA. The use of Eqs. (6) and (7) produce an error which is less than 1% in all cases. At 1310 nm, the error caused by variations in $\dot{f}$ is considered negligible, if $\dot{f}$ remains between 0.9 and 1. The total random error in SSA determination is therefore 8%. This estimate may seem optimistic in view of Fig. 5. However, a lot of the outlying points were obtained at an early stage of our work, before we had fully realized the impact of the state of the sample surface on reflectance, especially for samples with large grains. Subsequent measurements averaged a larger number of samples, reducing the random error.

The main systematic error is that of the CH_4 adsorption method. Legagneux et

al. (2002) estimated it at 10%, leading to an overall error of 12%. However, Kerbrat et al. (2007) showed that the CH_4 adsorption method gave results within 3% of X-ray tomography, so that it is reasonable to suggest that the systematic error due to CH_4 adsorption is 5% or less. In that case, the accuracy of SSA determination using IR reflectance at 1310 nm under the current conditions is then 10%.

5.2 Recommendation for snow with SSA>60 $m^2\,kg^{-1}$

For snow with SSA>60 $m^2\,kg^{-1}$, we recommend the use of 1550 nm radiation and the DISORT curves of Fig. 10, which shows that the beam collimation that determines $\dot{f}$ noticeably affects the location of the curve. We recommend to collimate the beam to obtain about an 8 mm spot on the snow, to illuminate a representative surface. With our 1550 nm Mitsubishi laser diode, $\dot{f}$ is then close to 0.87. To facilitate the use of Fig. 10, we propose the following polynomial fit, valid for 50<SSA<160 $m^2\,kg^{-1}$, with SSA in $m^2\,kg^{-1}$ and A_s in %:

$$\mathrm{SSA} = 0.07637A_s^2 + 8.480A_s + 11.55 \quad (8)$$

The error on this determination can be evaluated as above. Assuming that $\dot{f}$=0.87, the error du to SSA determination by CH_4 adsorption is here estimated to be 5% because of the lower number of points, the random error due to reflectance measurement is 2%, and the error due to crystal shape is again 3%, leading to a random error of 10%. If $\dot{f}$ is unknown within the range 0.81 to 0.94, the error rises top 12%. Using an estimate of systematic error of 5%, we evaluate the accuracy of SSA measurement using IR reflectance at 1550 nm to be 12% if $\dot{f}$ is known and 13% if $\dot{f}$ is unknown.

For the sake of completeness, we mention here the polynomial fit when $\dot{f}$=0.94:

$$\mathrm{SSA} = 0.07320A_s^2 + 8.636A_s + 11.78 \quad (9)$$

and for $\dot{f}$=0.81:

$$\mathrm{SSA} = 0.07923A_s^2 + 8.335A_s + 11.34 \quad (10)$$

Implicitly, the 60 $m^2\,kg^{-1}$ threshold suggests that the SSA of the snow must be evaluated before the measurement is made. This requirement is somewhat relaxed because both ranges overlap over the 50–66 $m^2\,kg^{-1}$ range. Moreover, in practice, a moderate amount of training and experience by a careful observer is sufficient to allow the visual estimation of SSA within about 20%. This was tested a number of times by writing down field estimates, subsequently compared to measurements.

6 Rapid and accurate determination of snow SSA in the field

We have successfully tested DUFISSS in both Alpine and Polar environments. As an illustration, Fig. 14 shows the stratigraphy, density and SSA profiles of an Alpine snow pit, studied on 7 February 2008 at a South facing site (45°02′09″ N, 6°24′02″ E) at an altitude of 2100 m near Col du Lautaret, French Alps. Once the stratigraphy had been observed and the instrument was in place, the SSA values were measured in about 30 min by two people. One was filling the sample holder with the snow using a core of the same diameter as the sample holder, weighted the sample holder to measure the density, and handed it to the other person who measured reflectance. Meanwhile, the first person was filling a second identical sample holder. SSA could not be measured at the very bottom of the snowpack because it was near 0°C and just handling the snow caused it to melt. However, careful observations indicated that the SSA of the 30 cm-thick bottom layer was homogeneous.

This stratigraphy allows the first determination of the snow area index (SAI) of an Alpine snowpack. The SAI has been defined by Taillandier et al. (2006), by analogy to the leaf area index (LAI) as the vertically integrated surface area of the snowpack. It is expressed in m^2 of snow surface area per m^2 of ground, and is therefore a dimensionless variable. It is computed as:

$$SAI_{snowpack} = \sum_i SSA_i h_i \rho_i \quad (11)$$

with h_i the height of layer i and ρ_i its density. We obtain SAI=5350, with an error of 15%. It is clear that the SAI of this Alpine snowpack is much greater than those of both Arctic (about 2500, Domine et al., 2002) and subarctic (about 1400, Taillandier et al., 2006) snowpacks. In fact, this 5350 SAI value is low for the alpine snowpack. This snowpack was subjected to many melting events, which reduced the SSA of most snow layers. We have measured SAI values in excess of 50,000 in colder areas, as will be detailed in subsequent publications.

7 Conclusions

DUFISSS allows the rapid determination of snow SSA in the field with an accuracy better than 13%. The principle, technology and use of DUFISSS are simple, and we therefore hope that it can soon be used in many studies by snow scientists who will apply it to chemical, climate, and snow physics research. As stated in the introduction, it can be used to study atmosphere-snow exchanges of chemicals (Burniston et al., 2007), especially right after snow falls, when SSA decreases rapidly. Hopefully it can also be used to help relate changes in snow radiative properties to snow physical properties, in particular in remote sensing studies. This may not be simple, however, because radiative properties measured in the field or derived from satellites are usually directional, not hemispherical, and complex BRDF considerations may be necessary. New approaches however appear promising (Zege et al., 2008). Finally, this rapid method will greatly facilitate the study of snow physics, and in particular the understanding of the factors affecting the rate of SSA changes, because in the past this has been limited by the small amount of data that could be obtained by CH_4 adsorption (Taillandier et al., 2007).

This method nicely complements those of Matzl and Schneebeli (2006) and of Painter et al. (2007). Both those methods are excellent to obtain the detailed stratigraphy of snowpacks, while our method is not designed for that useful purpose. On the other hand, and as detailed in the introduction, the shorter wavelengths used by those

authors imply that they will be difficult to use to obtain accurate values of snow SSA, especially for high SSA snows. Furthermore, it is possible that SSA determination at those wavelengths is affected by artifacts, potentially similar to those that we encountered. For example, Matzl and Schneebeli (2006) did observe that reflectance was different than expected by theory at high SSA. Interestingly, their measured reflectance is higher than theory, while our Fig. 3 shows the opposite, so that the explanation of their difference is uncertain at this stage. In summary, an ideal snow stratigraphic study will use the high resolution stratigraphic imaging proposed by those other authors, and the SSA measurement method proposed here.

Acknowledgements. DUFISSS was built without any external funds, despite repeated requests. We thank the LGGE director for his encouragements and support. We thank S. Aubert for hosting us at Station Alpine Joseph Fourier during our field study near Col du Lautaret. Ray-tracing calculations were made on the OSUG cluster maintained by F. Roch at Université Joseph Fourier, Grenoble. We thank L. Arnaud, E. Lefebvre and J.-P. Balestrieri for useful advice on several aspects of the instrumentation. CSZ was supported by NSF ARC-0714088 and NASA NNX07AR23G and acknowledges partial support from CNRS during his sabbatical year at LGGE.

CNRS CENTRE NATIONAL DE LA RECHERCHE SCIENTIFIQUE INSU The publication of this article is financed by CNRS-INSU.

References

Beine, H. J., Honrath, R. E. Domine, F. Simpson, W. R., and Fuentes J. D.: NO_x during background and ozone depletion periods at alert: fluxes above the snow surface, J. Geophys. Res., 107(D21), 4584, doi:10.1029/2002JD002082, 2002.

Burniston, D. A., Strachan, W. J. M., Hoff, J. T., and Wania, F.: Changes in surface area and concentrations of semivolatile organic contaminants in aging snow, Environ. Sci. Technol., 41, 4932–4937, 2007.

Cabanes, A., Legagneux, L., and Domine, F.: Evolution of the specific surface area and of crystal morphology of Arctic fresh snow during the ALERT 2000 campaign, Atmos. Environ., 36, 2767–2777, 2002.

Cabanes, A., Legagneux, L., and Domine, F.: Rate of evolution of the specific surface area of surface snow layers, Environ. Sci. Technol., 37, 661–666, 2003.

Coakley, J.A, Cess, R. D., and Yurevich, F. B.: The effect of tropospheric aerosols on the Earth's radiation budget: a parameterization for climate models, J. Atmos. Sci., 40, 116–138, 1983.

Colbeck, S. C.: Ice crystal morphology and growth rates at low supersaturations and high temperatures, J. Appl. Phys., 54, 2677–2682, 1983.

Daly, G. L. and Wania, F.: Simulating the influence of snow on the fate of organic compounds, Environ. Sci. Technol., 38, 4176–4186, 2004.

Davis, R. E., Dozier, J., and Perla, R.: Measurement of snow grain properties. In: Seasonal Snowcovers: Physics, Chemistry, Hydrology, edited by: Jones, H. G., and Orville-Thomas, W. J., D. Reidel Publishing Dompany, 63–74, 1987.

Domine, F. and Shepson, P. B.: Air-snow interactions and atmospheric chemistry, Science, 297, 1506–1510, 2002.

Domine, F., Cabanes, A., and Legagneux, L.: Structure, microphysics, and surface area of the Arctic snowpack near Alert during ALERT 2000, Atmos. Environ. 36, 2753–2765, 2002.

Domine, F., Lauzier, T., Cabanes, A., Legagneux, L. Kuhs, W. F., Techmer, K., and Heinrichs, T.: 2003 snow metamorphism as revealed by scanning electron microscopy, Microsc. Res. Tech., 62, 33–48, 2003.

Domine, F., Salvatori, R., L. Legagneux, L., Salzano, R., Fily M., and Casacchia, R.: Correlation between the specific surface area and the short wave infrared:SWIR reflectance of snow, Cold Regions Sci. Technol., 46, 60–68, doi:10.1016/j.coldregions.2006.06.002, 2006.

Domine, F., Taillandier, A.-S., and Simpson W. R.: A parameterization of the specific surface area of snow in models of snowpack evolution, based on 345 measurements, J. Geophys. Res., 112, F02031, doi:10.1029/2006JF000512, 2007a.

Domine, F., Cincinelli, A., Bonnaud, E., Martellini, T., and Picaud, S.: Adsorption of phenanthrene on natural snow, Environ. Sci. Technol., 41, 6033–6038, 2007.

Domine, F., Albert, M., Huthwelker, T., Jacobi, H.-W., Kokhanovsky, A. A., Lehning, M., Picard, G., and Simpson, W. R.: Snow physics as relevant to snow photochemistry, Atmos. Chem. Phys., 8, 171–208, 2008, http://www.atmos-chem-phys.net/8/171/2008/.

Flanner, M. G. and Zender, C. S.: Linking snowpack microphysics and albedo evolution, J. Geophys. Res., 111, D12208, doi:10.1029/2005JD006834, 2006.
Flin, F., Brzoska, J.-B., Lesaffre, B., Coléou, C., and Pieritz, R. A.: Full three-dimensional modelling of curvature-dependent snow metamorphism: first results and comparison with experimental tomographic data, J. Phys. D. Appl. Phys., 36, 1–6, 2003.
Gosse, S., Labrie, D., and Chylek, P.: Refractive index of ice in the 1.4–7.8-µm spectral range, Appl. Opt., 34, 6582–6586, 1995.
Grannas, A. M., Jones, A. E., Dibb, J., Ammann, M., Anastasio, C., Beine, H. J., Bergin, M., Bottenheim, J., Boxe, C. S., Carver, G., Chen, G., Crawford, J. H., Domine, F., Frey, M. M., Guzmán, M. I., Heard, D. E., Helmig, D., Hoffmann, M. R., Honrath, R. E., Huey, L. G., Hutterli, M., Jacobi, H. W., Klán, P., Lefer, B., McConnell, J., Plane, J., Sander, R., Savarino, J., Shepson, P. B., Simpson, W. R., Sodeau, J. R., von Glasow, R., Weller, R., Wolff, E. W., and Zhu, T.: An overview of snow photochemistry: evidence, mechanisms and impacts, Atmos. Chem. Phys., 7, 4329–4373, 2007, http://www.atmos-chem-phys.net/7/4329/2007/.
Grenfell, T. C., Warren, S. G., and Mullen, P. C.: Reflection of solar radiation by the Antarctic snow surface at ultraviolet, visible, and near-infrared wavelengths, J. Geophys. Res., 99, 18 669–18 684, 1994.
Grenfell, T. C. and Warren, S. G.: Representation of a nonspherical ice particle by a collection of independent spheres for scattering and absorption of radiation, J. Geophys. Res., 104, 31 697–31 709, 1999.
Hall, A.: The role of surface albedo feedback in climate, J. Climate, 17, 1550–1568, 2004.
Herbert, B. M. J., Halsall, C. J., Villa, S., Jones, K. C., and Kallenborn, R.: Rapid changes in PCB an OC pesticide concentrations in Arctic snow, Environ. Sci. Technol., 39, 2998–3005, 2005.
Hidović-Rowe, D., Rowe, J. E., and Lualdi, M.: Markov models of integrating spheres for hyperspectral imaging, Appl. Opt., 45, 5248–5257, 2006.
Honrath, R. E., Peterson, M. C., Guo, S., Dibb, J. E., Shepson, P. B., and Campbell, B.: Evidence of NO_x production within or upon ice particles in the Greenland snowpack, Geophys. Res. Lett., 26, 695–698, 1999.
Jacobi, H.-W. and Hilker, B.: A mechanism for the photochemical transformation of nitrate in snow, J. Photochem. Photobiol. A., 185, 371–382, 2007.
Jones, A. E., Weller, R., Anderson, P. S., Jacobi, H.-W., Wolff, E. W., Schrems, O., and Miller, H.:

Measurements of NO_x emissions from the Antarctic snowpack, Geophys. Res. Lett., 28, 1499–1502, 2001.
Kerbrat, M., Pinzer, B., Huthwelker, T., Gäggeler, H. W., Ammann, M., and Schneebeli, M.: Measuring the specific surface area of snow with X-ray tomography and gas adsorption: comparison and implications for surface smoothness, Atmos. Chem. Phys., 8, 1261–1275, 2008, http://www.atmos-chem-phys.net/8/1261/2008/.
Kokhanovsky, A. A.: Scaling constant and its determination from simultaneous measurements of light reflection and methane adsorption by snow samples, Opt. Lett., 31, 3282–3284, 2006.
Legagneux, L., Cabanes, A., and Domine, F.: Measurement of the Specific Surface Area of 176 Snow Samples Using Methane Adsorption at 77 K, J. Geophys. Res., 107(D17), 4335, doi:10.1029/2001JD001016, 2002.
Matzl, M. and Schneebeli, M.: Measuring specific surface area of snow by near-infrared photography, J. Glaciol., 52, 558–564, 2006.
Narita, H.: Specific surface of deposited snow II, Low Temp. Sci. A., 29, 69–81, 1971.
Nolin, A. W. and Dozier, J.: A hyperspectral method for remotely sensing the grain size of snow, Remote Sens. Environ., 74, 207–216, 2000.
Nelson, J.: Sublimation of ice crystals, J. Atmos. Sci., 55, 910–919, 1998.
Painter, T. H., Molotch, N. P., Cassidy, M., Flanner, M., and Steffen, K.: Contact Spectroscopy for Determination of Stratigraphy of Optical Grain Siz, J. Glaciol., 53, 121–127, 2007.
Perla, R., Dozier, J., and Davis, R. E.: Preparation of serial sections in dry snow specimens, J. Microsc., 141, 111–114, 1986.
Picard, G., Arnaud, L., Domine, F., and Fily, M.: Determining snow specific surface area from near-infrared reflectance measurements: numerical study of the influence of grain shape, Cold Regions Sci. Technol., in press, 2008.
Pickering, J. W., Prahl, S. A., Vanwieringen, N., Beek, J. F., Sterenborg, H. J. C. M., and Vangemert, M. J. C.: Double-integrating-sphere system for measuring the optical properties of tissue, Appl. Opt., 32, 399–410, 1993.
Stamnes, K., Tsay, S. C., Wiscombe, W., and Jayaweera, K.: Numerically stable algorithm for discrete-ordinate-method radiative transfer in multiple scattering and emitting layered media, Appl. Opt, 27, 2502–2509, 1988.
Taillandier, A.-S., Domine, F., Simpson, W. R., Sturm, M., Douglas, T. A., and Severin, K.: Evo-

lution of the Snow Area Index: SAI of the subarctic snowpack in Central Alaska over a whole season. Consequences for the air to snow transfer of pollutants, Environ. Sci. Technol., 40, 7521–7527, doi:10.1021/es060842j, 2006.

Taillandier, A.-S., Domine, F., Simpson, W. R., Sturm, M., and Douglas, T. A.: The rate of decrease of the specific surface area of dry snow: isothermal versus temperature gradient conditions, J. Geophys. Res., 112, F03003, doi:10.1029/2006JF000514, 2007.

Warren, S. G.: Optical properties of snow, Rev. Geophys. Space Phys., 20, 67–89, 1982.

Warren, S. G.: Optical constants of ice from the ultraviolet to the microwave, Appl. Opt., 23, 1206–1225, 1984.

Warren, S. G. and Brandt, R. E.: Optical constants of ice from the ultraviolet to the microwave: a revised compilation, J. Geophys. Res., 113, D14220, doi:10.1029/2007JD009744, 2008.

Wiscombe, W. J. and Warren, S. G.: A model for the spectral albedo of snow. I: Pure snow, J. Atmos. Sci. 37, 2712–2733, 1980.

Zege, E., Katsev, I., Malinka, A., Prikhach, A., and Polonsky, I.: New algorithm to retrieve the effective snow grain size and pollution amount from satellite data, Ann. Glaciol., 49, 139–144, 2008.

Zender, C. S. and Talamantes, J.: Solar absorption by Mie resonances in cloud droplets, J. Quant. Spectrosc. Ra., 98, 122–129, doi:10.1016/j.jqsrt.2005.05.084, 2006.

Table 1. Reflectances at 1310 nm of experimental snow samples with high SSA and low density, compared to calculations using DISORT that test the effect of density, and to calculations that account for the geometric artifact. $\dot{f}$=0.95 was used in all the calculations.

Measured SSA, $m^2\,kg^{-1}$	Measured density $kg\,m^{-3}$	Sample holder depth, mm	Measured reflectance, %	Calculated reflectance %, actual density	Calculated reflectance %, density= $400\,kg\,m^{-3}$	Reflectance with actual density and geometric artifact, %
131.3	35	25	52.2	65.21	66.05	60.89
112.7	36	25	53.1	62.60	63.69	58.08
108.6	35	25	49.5	61.89	63.23	57.16
97.7	109	13	53.7	61.26	61.48	59.57
77.3	169	13	53.0	57.64	57.68	55.30

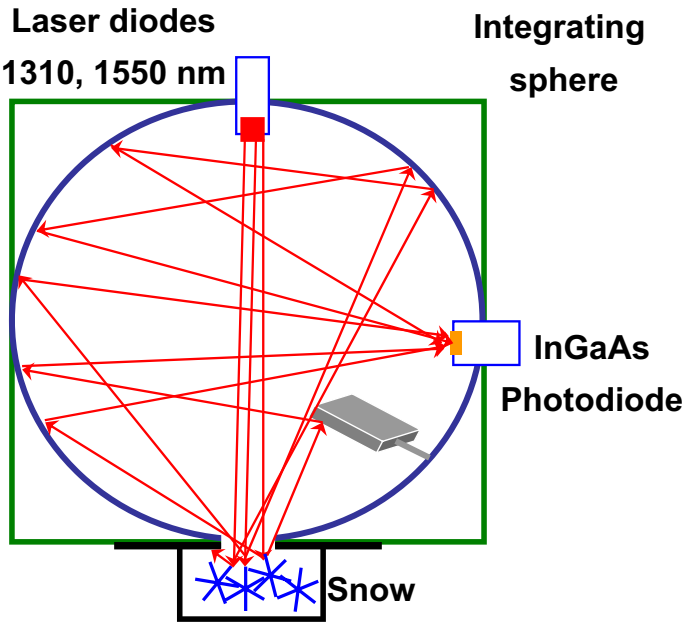

Fig. 1. DUFISSS: integrating sphere developed for the measurement of the specific surface area of snow. Direct reflection from the snow to the photodiode is blocked by an optical baffle.

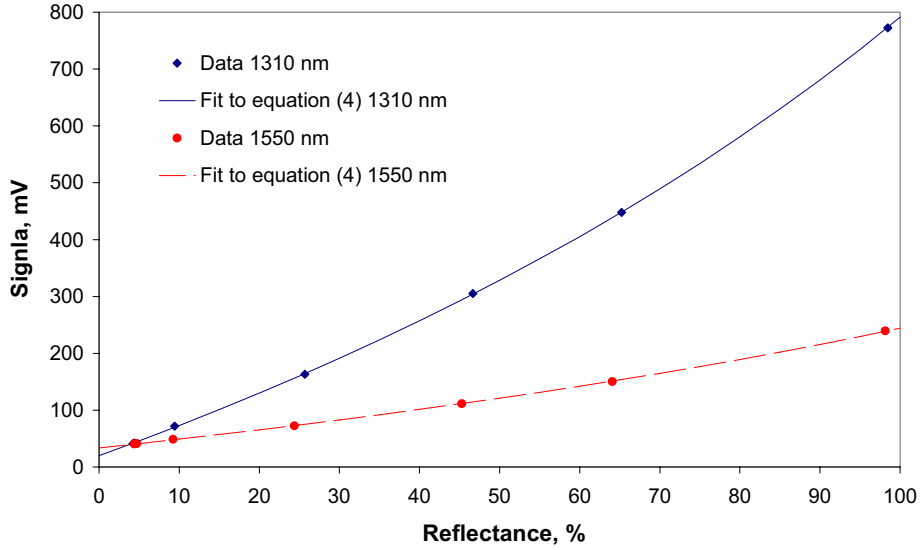

Fig. 2. Calibration curves used to determine snow reflectance from the photodiode signals. Graphite-doped Zenith® reflectance standards were used. The curves are not linear because of the reillumination of the standards by their reflected light. The fit to the points was made using Eq. (4), where $\dot{f}=0.962$ at 1310 nm and $\dot{f}=0.807$ at 1550 nm.

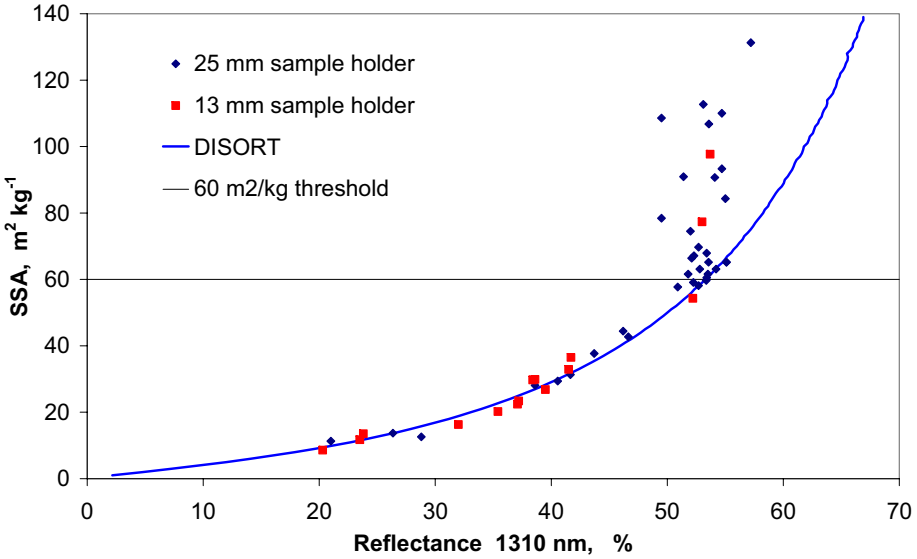

Fig. 3. Calibration curve to determine snow specific surface area from reflectance at 1310 nm measured with the integration sphere. Specific surface area was measured by CH_4 adsorption at 77 K. Reflectance was obtained with snow samples contained either in a 13 or a 25 mm deep sample holder. Reflectance was also calculated using the DISORT model, for 25 mm thick snow samples of density 400 kg m^{-3}, with $\acute{f}$=0.95, over a surface with 6% reflectance. For snow with SSA above 66 m^2 kg^{-1}, the scatter and deviation from DISORT calculations are caused by the artifacts detailed in Fig. 4. The line at SSA=60 m^2 kg^{-1} indicates that above that line, snow usually has a low density and the use of this calibration may lead to large errors. Below SSA=1 m^2 kg^{-1}, Mie theory breaks down and calculations are not possible.

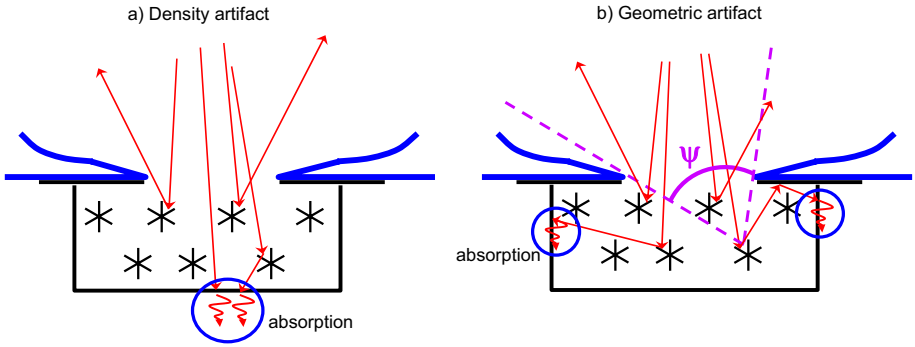

Fig. 4. Two artifacts detected in our system that lower snow reflectance. **(a)** in low density snow, light penetrates sufficiently deep in the snow that it can reach the bottom of the sample holder, where it is absorbed. **(b)** light scattered by reflectors below the surface has a reduced probability of escaping, because its field of view is limited by angle ψ.

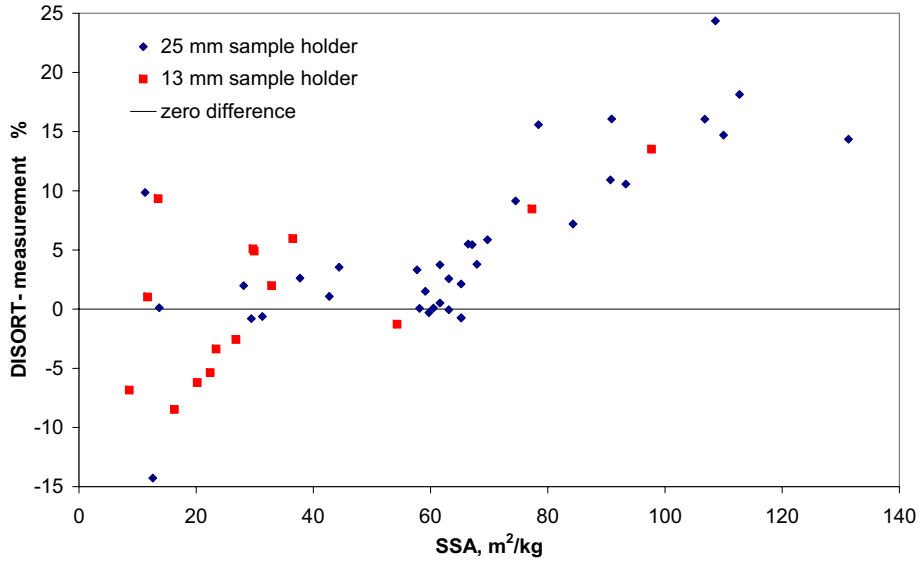

Fig. 5. Difference in reflectance, for given SSA values, between the calculations by DISORT and our measured value. DISORT uses snow with a density of 400 kg m^{-3}. The systematically lower value of our measurement for SSA>66 m^2 kg^{-1} appears clearly. The lowest point on the graph, at SSA=12.6 m^2 kg^{-1}, was a melt-freeze crust whose rough surface certainly affected the measurement quality.

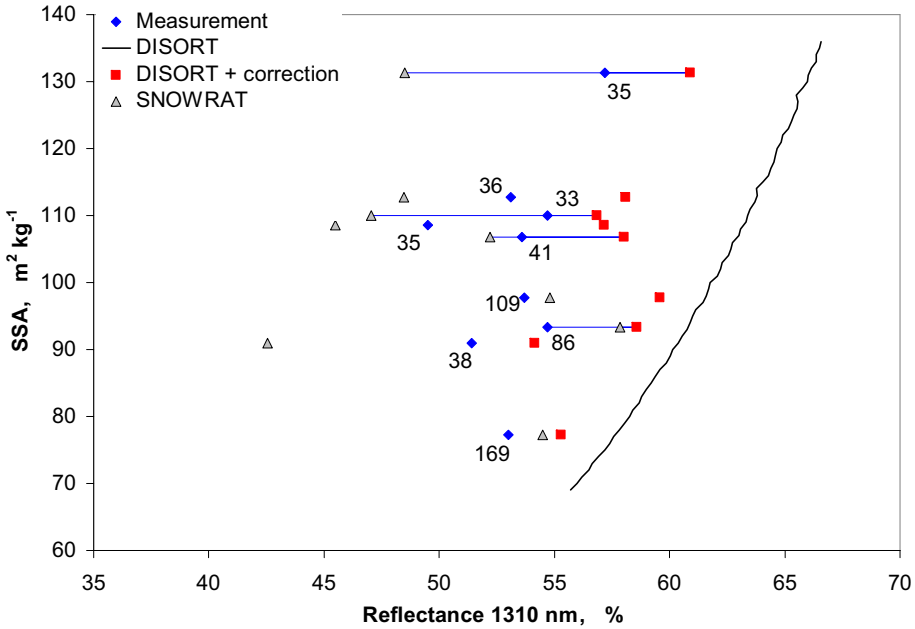

Fig. 6. Reflectance at 1310 nm of snow samples whose SSA was measured using CH_4 adsorption at 77 K. Three methods were used to obtain reflectance: measurement with the integration sphere, calculation using DISORT with geometric corrections using Eq. (5), and the ray-tracing model SNOWRAT. For each snow sample, there are therefore 3 reflectance values, some of which are connected by blue lines for clarity. The numbers next to each measured value is the mean density of the snow sample in the sample holder, in kg m^{-3}. The SSA-Reflectance relationship using DISORT without correction, for snow of density 400 kg m^{-3} and with $\dot{f}$=0.95, is also shown.

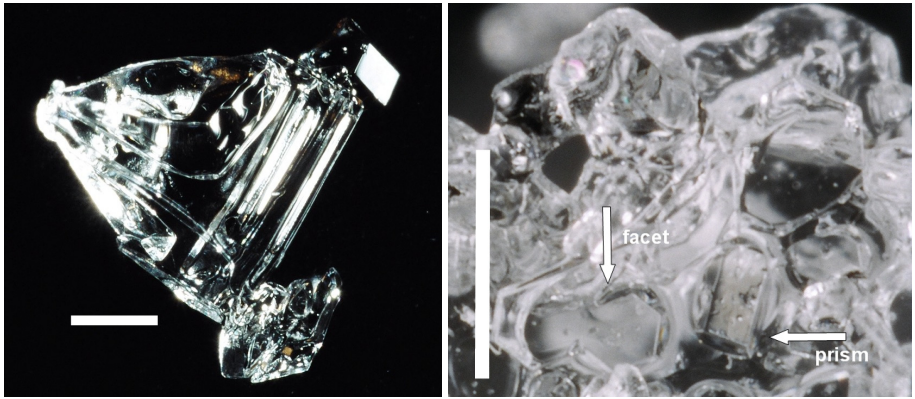

Fig. 7. Left: depth hoar cristal, showing the coexistence of faceted and rounded shapes. Right: melt-freeze crust, showing faceted shapes, even though melt-freeze crust are often thought to consist only of rounded shapes. Scale bars: 1 mm.

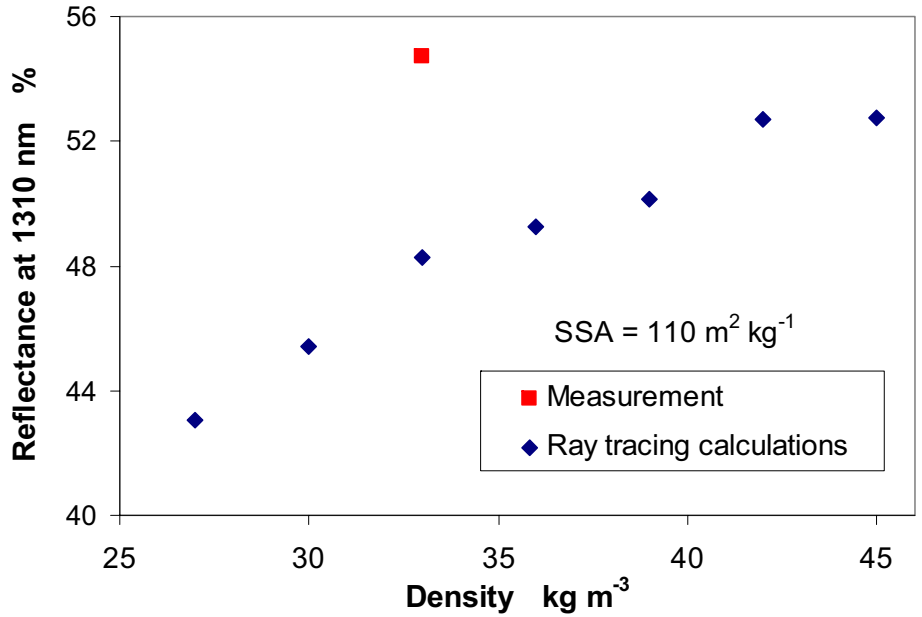

Fig. 8. Effect of snow density on reflectance at 1310 nm for low density – high SSA snows, as calculated by SNOWRAT for our integration sphere with illumination at 1310 nm. The model uses disconnected spheres having an SSA of 110 $m^2\,kg^{-1}$. The curve is not perfectly smooth because of numerical noise. The measured reflectance of a snow sample of the same SSA is also shown.

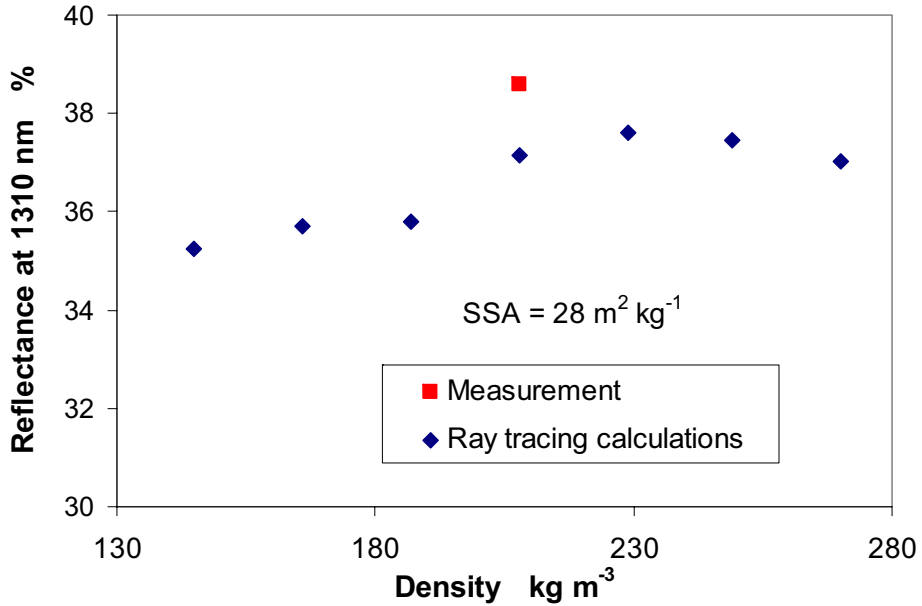

Fig. 9. Effect of snow density on reflectance at 1310 nm for snows of moderate densities and of SSA=28 $m^2\,kg^{-1}$, as calculated by SNOWRAT for our integration sphere with illumination at 1310 nm. As in Fig. 8, the curve is not perfectly smooth because of numerical noise. The measured reflectance of a snow sample of SSA=28.1 $m^2\,kg^{-1}$ is also shown.

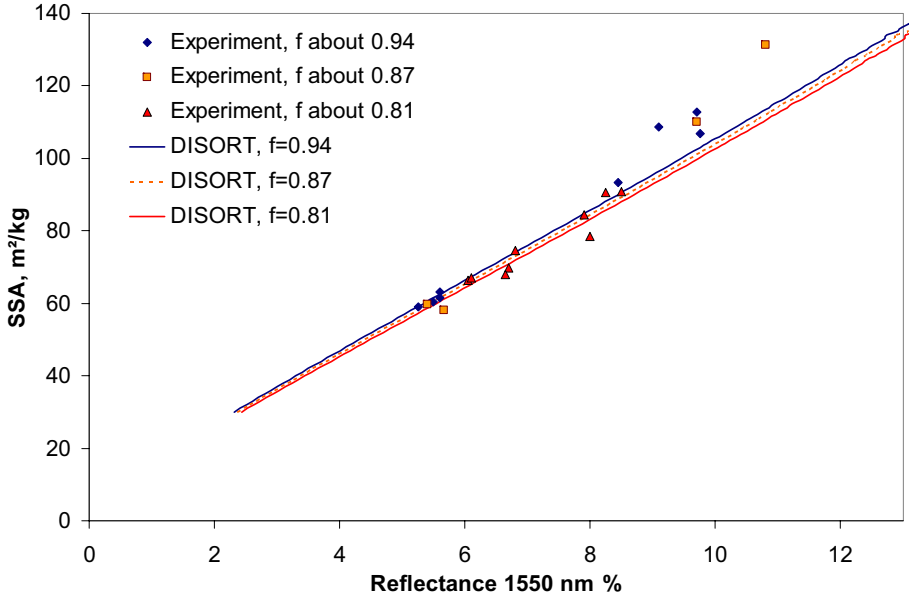

Fig. 10. Calibration curve to determine snow specific surface area from reflectance at 1550 nm measured with DUFISSS. Specific surface area was measured by CH_4 adsorption at 77 K. Reflectance was obtained with snow samples contained in a 25 mm-deep sample holder. Reflectance was also calculated using the DISORT model, for 25 mm-thick snow samples of density 400 kg m^{-3}, over a surface with 6% reflectance. Measurements and calculations were performed for 3 values of $\dot{f}$.

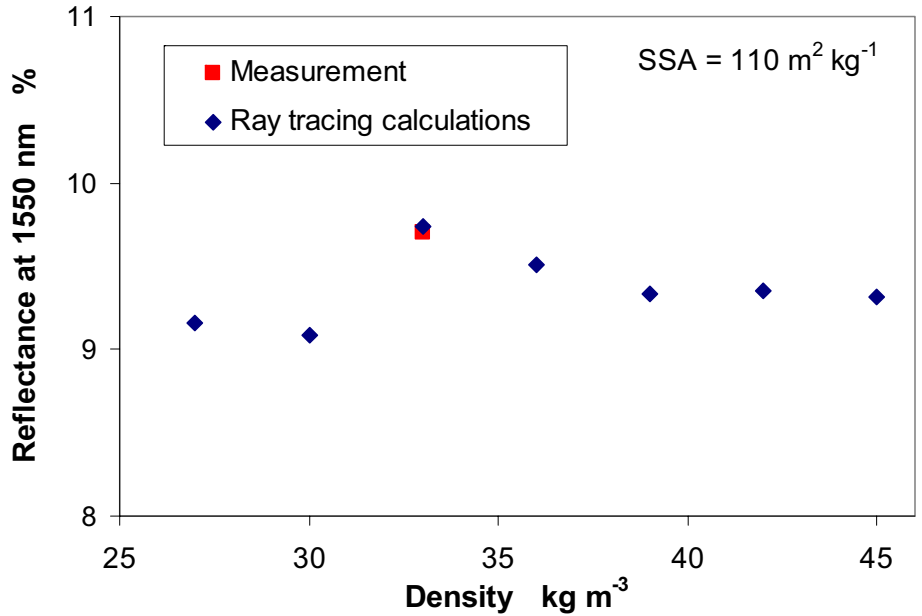

Fig. 11. Effect of snow density on reflectance at 1550 nm for low density – high SSA snows, as calculated by SNOWRAT for our integration sphere with illumination at 1550 nm. The model uses disconnected spheres having an SSA of 110 $m^2\,kg^{-1}$. The curve is not perfectly smooth because of numerical noise. The measured reflectance of a snow sample of the same SSA is also shown.

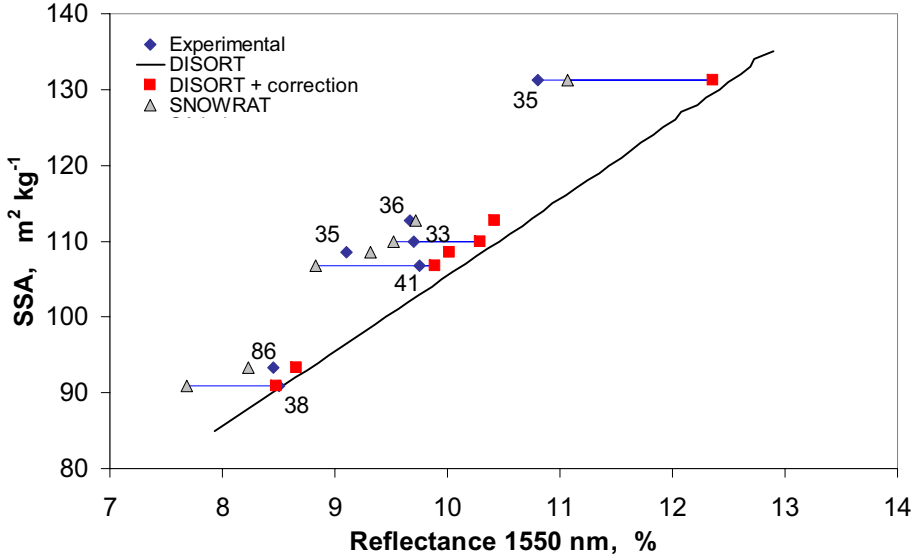

Fig. 12. Reflectance at 1550 nm of snow samples whose SSA was measured using CH_4 adsorption at 77 K. Three methods were used to obtain reflectance: measurement with the integration sphere, calculation using DISORT with geometric corrections using Eq. (5), and SNOWRAT. For each snow sample, there are therefore 3 reflectance values, some of which are connected by blue lines for clarity. The numbers next to each measured value is the mean density of the snow sample in the sample holder, in kg m^{-3}. The SSA-Reflectance relationship using DISORT without correction, with $\dot{f}$=0.94, is also shown.

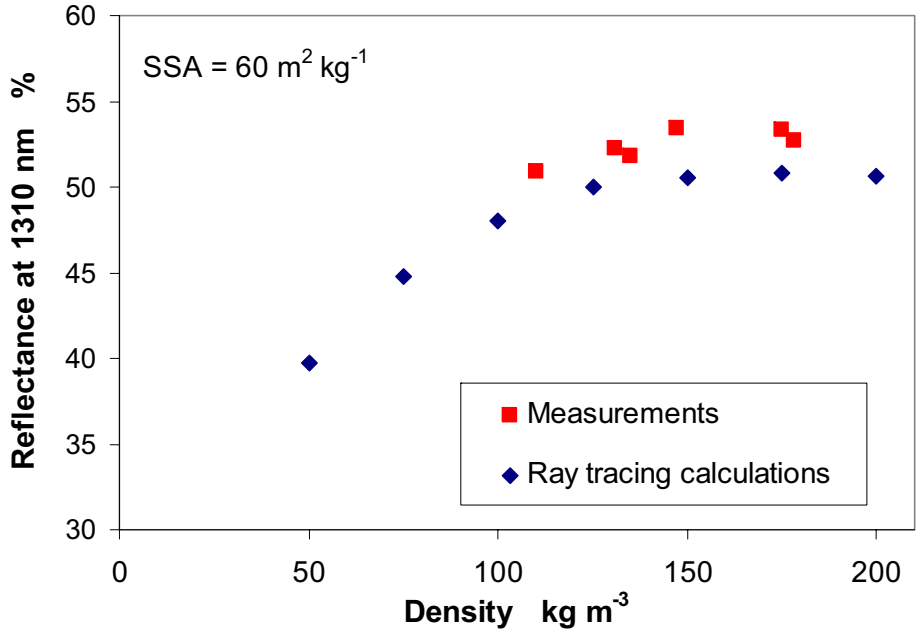

Fig. 13. Effect of snow density on reflectance at 1310 nm for snows of low to moderate densities and moderately high SSA, as calculated by SNOWRAT for DUFISSS. The model uses disconnected spheres having an SSA of 60 $m^2\ kg^{-1}$. The measured reflectances of snow samples having SSAs in the range 57–63 $m^2\ kg^{-1}$ are also shown.

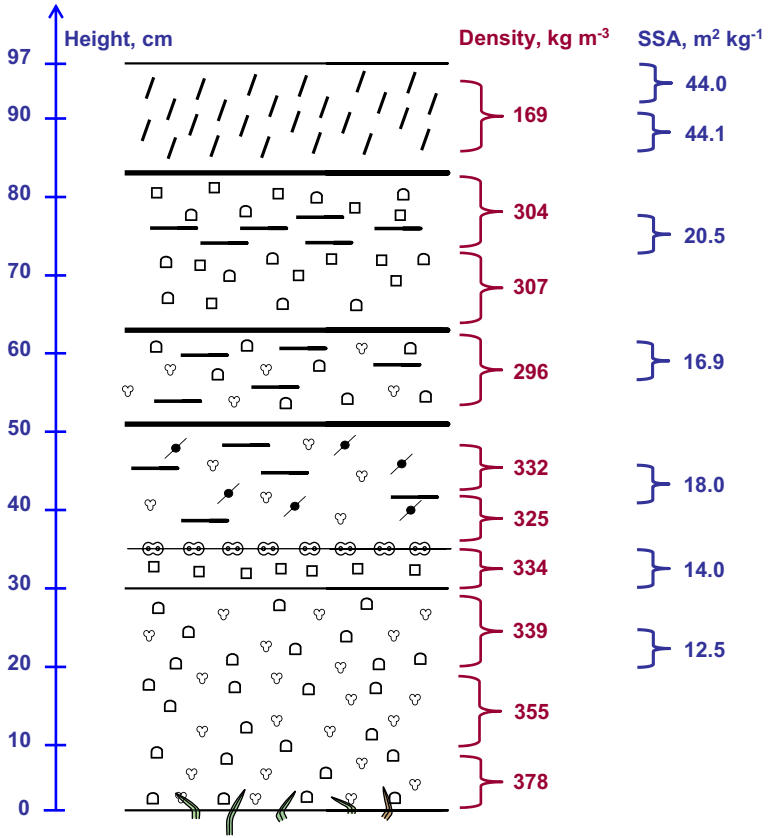

Fig. 14. Stratigraphy of the Alpine snowpack near Col du Lautaret, French Alps, on 7 February 2008, showing the SSA measured by DUFISSS and the density of the main snow layers.